

Supporting Information for

Facile fabrication of N/S- doped carbon nanotubes with Fe₃O₄ nanocrystals enched for lasting synergy as efficient oxygen reduction catalysts

Shanshan Zeng ^{a,b}, Fucong Lyu ^{a,c,d}, Hongjiao Nie ^{a,b}, Yawen Zhan ^{a,b}, Haidong Bian ^{a,b}, Yayuan Tian ^{a,b},
Zhe Li ^{a,b}, Aiwu Wang ^{a,b}, Jian Lu ^{c,d,*}, Yang Yang Li ^{a,b,e,*}

Table of Contents

- Experimental details
- Figure S1. Digital images of the mass production
- Figure S2. XRD pattern of NSCNT-800
- Figure S3. Raman spectra of NSCNT-800 and Fe-NSCNT fabricated at different annealing temperature
- Figure S4. SEM images of as-prepared Fe-PPy-MO and PPy-MO
- Figure S5. SEM images of Fe-PPy-MO and PPy-MO after 500 °C annealing
- Figure S6. SEM images of NSCNT-800
- Figure S7. TEM images of NSCNT-800
- Figure S8. LSV curves of Fe-NSCNT-700, Fe-NSCNT-800 and Fe-NSCNT-900
- Figure S9. LSV curves and corresponding Koutecky-Levich plots of Fe-NSCNT-700 and Fe-NSCNT-900
- Figure S10. LSV curves and corresponding Koutecky-Levich plots of NSCNT-800
- Figure S11. Comparison of electron transfer number and kinetic limiting current density
- Figure S12. Loading test of ORR performance of Fe-NSCNT-800
- Figure S13. Percentage of peroxide and the electron transfer number of Fe-NSCNT-800 and NSCNT-800
- Figure S14. LSV curves of Fe-NSCNT-800 and Fe-NC-800
- Figure S15. TEM images of Fe-NSCNT-800 after stability test

- Figure S16. ORR performance of the catalysts in acid solution
- Figure S17. Schematic components diagram of the home-built Zinc-air cell
- Figure S18. OCV of Zn-air batteries constructed using Fe-NSCNT-800 and 20% Pt/C

Experimental

Materials fabrication

In a typical procedure, 5 mmol methyl orange (MO) was dissolved in 30 mL deionized water, followed by the addition of 1.5 mmol FeCl₃ with stirring. A rufous flocculent precipitate formed immediately. Then, 105 μ L pyrrole monomer (Aldrich) was added, and the mixture was stirred at room temperature for 24 h for producing hybrids polypyrrole nanotubes and methyl orange (denoted as “PPy-MO”). After that, 50 ml 0.5 M NaOH was added to the above suspension for in-situ precipitation of Fe₃O₄ inside the PPy-MO. The precipitate (denoted as “Fe-PPy-MO”) was filtered, washed with deionized water/ethanol, and dried in vacuum at 60 °C for 24 h.

The as-prepared Fe-PPy-MO was thoroughly grounded into fluffy powders, transferred into a lidded ceramic boat, and underwent pyrolysis at 500 °C for 2 h in Ar (the thus obtained precursor is denoted as “Fe-NSCNT-precursor”). The cooled sample in the form of black powders was then immersed in 6 M HCl solution for 12 h to remove the superfluous Fe species. After washing and drying, the powders were heated in Ar for 5 h at 800 °C (700 °C and 900 °C also tested, treated sample denoted as “Fe-NSCNT-T” with T representing the annealing temperature). The control sample (denoted as “NSCNT-800”) was synthesized following the same procedure, but without NaOH treatment to precipitate Fe₃O₄.

Materials characterizations

The morphology of the as-prepared samples were investigated using scanning electron microscopy (SEM, Philips XL-30 FESEM), and transmission electron microscopy (TEM, JEOL TEM 2100F FEG operated with an accelerating voltage of 200 kV). Raman spectrum was conducted with a Renishaw-200 visual Raman microscope (633nm in wavelength). The X-ray diffraction (XRD) patterns were collected using an X-ray diffractometer (Rigaku SmartLab) using Cu K α radiation. Brunauer-Emmett-Teller (BET) surface area were tested on a Micromeritics, ASAP2020 gas sorption analyzer at 77 K. X-ray photoelectron spectroscopy (XPS) measurements were carried out on a VG ESCALAB 220i-XL surface analysis system.

Oxygen reduction reaction test

4 mg catalyst was dispersed in 400 μ L of 0.5 wt% Nafion ethanol solution ultrasonically to form homogeneous slurry. The slurry (8 μ L) was then transferred onto a glassy carbon electrode with a catalyst loading of 409 μ g cm⁻². Prior to use, the glassy carbon electrode (GCE, 0.19625 cm²) was sequentially polished with a 0.05 μ m alumina slurry and then washed ultrasonically in water and ethanol (30 s each), the cleaned electrode was dried with a high-purity nitrogen steam. The catalyst-coated glassy carbon electrode, Hg/HgO (KOH, 0.1 M) or saturated calomel electrode (SCE) (H₂SO₄, 0.5 M), and Pt wire were used as the working, reference and counter electrode, respectively. Electrochemical measurements were conducted on a Biologic VMP3 electrochemical station with a flowing gas three-electrode cell system at room temperature. For comparison, the commercial Pt/C powder was purchased from Alfa Aesar and tested with the same loading of 409 μ g cm⁻².

All the electrochemical experiments were performed in O₂- or Ar- saturated 0.1 M KOH (0.5 M H₂SO₄) electrolyte. Cyclic voltammograms (CVs) were performed between -0.8 and +0.2 V *versus* Hg/HgO in 0.1 M KOH (or between -0.4 and 0.7 V *versus* SCE in 0.5 M H₂SO₄), at a scan rate of 10 mV s⁻¹. The rotating disk electrode (RDE) ($\varphi = 5$ mm, 0.19625 cm²) was investigated at different rotating speed from 400 to 2500 rpm, and the rotating ring-disc electrode (RRDE) at 1600 rpm.

The slopes of their best linear fit lines of the samples after background correction were used to calculate the number of electrons transferred (n) on the basis of the Koutecky-Levich equations (eqs. 1-3):

$$\frac{1}{J} = \frac{1}{J_L} + \frac{1}{J_K} = \frac{1}{B\omega^{1/2}} + \frac{1}{J_K} \quad (1)$$

$$B = 0.62nFC_0(D_0)^{2/3}\nu^{-1/6} \quad (2)$$

$$J_K = nFkC_0 \quad (3)$$

where J , J_K , J_L are the measured current density, kinetic and diffusion limiting current densities, respectively, ω is the angular velocity of the disk, B is the reciprocal of the slope, which can be determined from the slope of K-L plot using Levich equation, n is the electron transferring number, F is the Faraday constant (96485 C mol⁻¹), C_0 is the bulk concentration of O₂, D_0 is the diffusion coefficient of O₂, ν is the viscosity of the electrolyte, and k is the electron transfer rate constant.

The % HO₂⁻ and the electron transfer number (n) were determined by the the following equations (eqs. 4-5):

$$\%HO_2^- = 200 \times \frac{I_r/N}{I_d+I_r/N} \quad (4)$$

$$n = 4 \times \frac{I_d}{I_d + I_r / N} \quad (5)$$

Where $N = 0.37$ is the collection efficiency which is reported by the manufacturer for the setup, I_d and I_r are the disk and ring current, respectively.

All the experiments were carried out at room temperature. The loading $407 \mu\text{g cm}^{-2}$ was chosen since it is the loading experimentally employed for being closed to the most active catalysts with a lower usage amount of catalyst in RDE (as showed in Figure S12). All experiment were carried out in this loading unless special illustration. All potentials were later converted to the RHE scale, for Hg/HgO reference in alkaline condition, $V_{\text{RHE}} = V_{\text{Hg/HgO}} + V_{\text{Hg/HgO}}^{\theta} + 0.059\text{pH} = V_{\text{Hg/HgO}} + 0.932$; for SCE reference in acid condition, $V_{\text{RHE}} = V_{\text{SCE}} + V_{\text{SCE}}^{\theta} + 0.059\text{pH} = V_{\text{SCE}} + 0.259$.

Zinc–air battery tests

The measurements of the zinc–air batteries were performed using home-built electrochemical cells, as showed in Figure S1. Amounts of 5 mg of catalysts was dissolved in 900 μL of distilled water and 100 μL of Nafion ethanol solution (5 wt% in ethanol) and ultrasonicated for 60 min to achieve a homogenized ink (5 mg mL^{-1}). To obtain a loading of 1 mg cm^{-2} , 200 μL of the ink was uniformly drop-coated onto Teflon-treated carbon fiber paper (AvCarb P75T, Fuel Cell Store) as the gas diffusion layer with a geometric area of 1.0 cm^2 . We used water here instead of ethanol to mix with Nafion solution is that the water can't diffuse through the carbon paper so that the ink can dry gradually under heating and form a homogeneous catalyst film in the well design region on the carbon paper. A Zn foil ($2.5 \text{ cm} * 2 \text{ cm} * 0.3 \text{ mm}$) was first polished to serve as the anode. The zinc–air

battery was fabricated by pairing the air cathode and zinc anode in 28 ml of 6 M KOH. The cathode shell of the home-made cell has a big bent to let the air contact the air cathode directly, and a piece of nickel foam was assembled between the cathode shell and the air cathode as a buffer layer and current conductor. With these design, the air can easily reach carbon air cathode and diffuse through the carbon paper which serve as diffusion layer and current collector and finally be converted by catalyst. Linear sweep voltammetry (LSV) was conducted within a range of 1.6 V – 0.4 V at 5 mV s⁻¹ using a potentiostat (CHI 660E). Galvanostatic discharge experiments of the zinc air cells were conducted using a Neware automatic battery cyler at several different rates under different current densities.

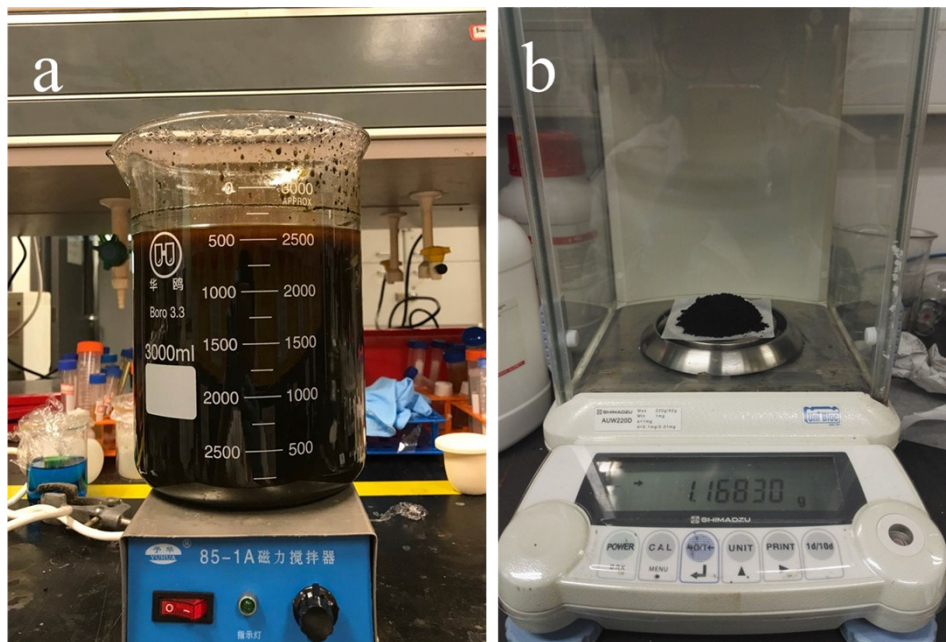


Figure S1. Photographs of the reaction solution (a), and final product from the scale-up synthesis (b).

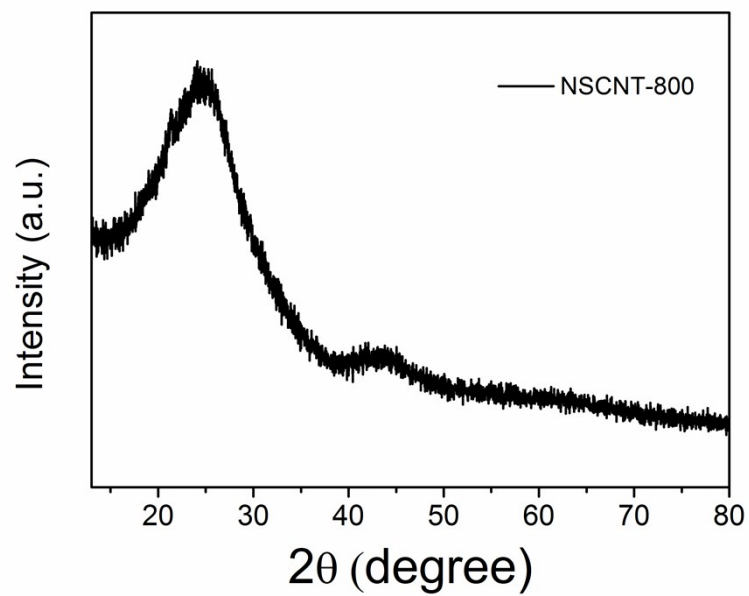


Figure S2. XRD pattern of NSCNT-800.

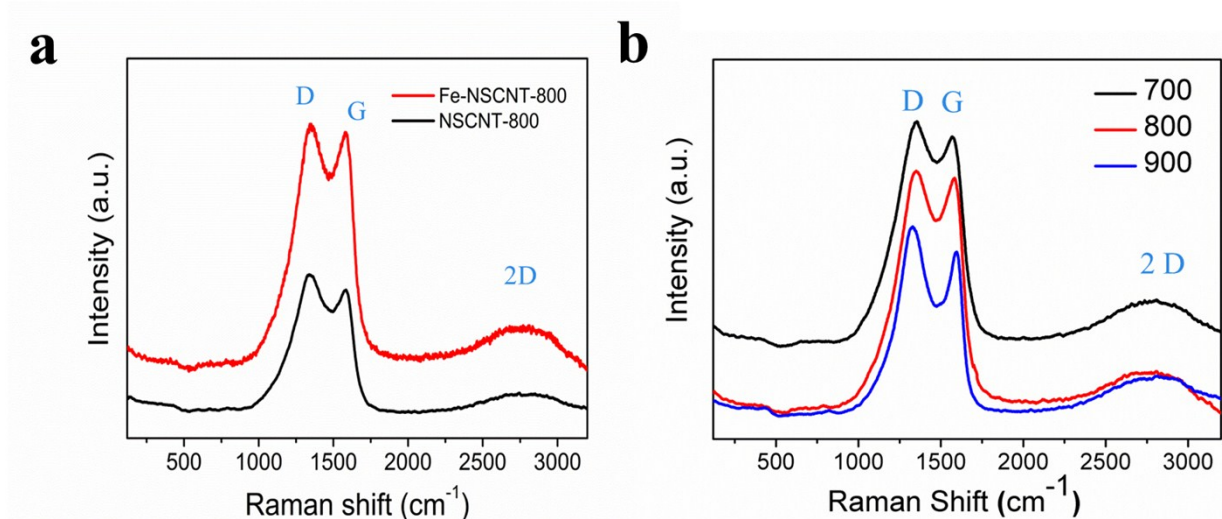


Figure S3. Raman spectra of Fe-NSCNT-800 and NSCNT-800 (a) and Fe-NSCNT-700, Fe-NSCNT-800 and Fe-NSCNT-900 (b).

The I_G/I_D increases with the increase of pyrolysis temperature and reaches a maximum value of 0.95 at a temperature of 800 °C, indicating the higher graphitic crystallinity and more defects of the carbon structures for Fe-NSCNT-800. Different from the common observation in literature that the carbon structure becomes more ordered with increased pyrolysis temperature, I_D/I_G of Fe-NSCNT-900 decreases to 0.86, possibly because more heteroatoms are incorporated into the carbon structures when annealed at 900 °C lowering the structural orders. Moreover, compared with NSCNT-800 ($I_D/I_G=0.9$ and lower 2D peak), Fe-NSCNT-800 possesses a higher degree of graphitic ordering and thus higher conductivity, beneficial for ORR.

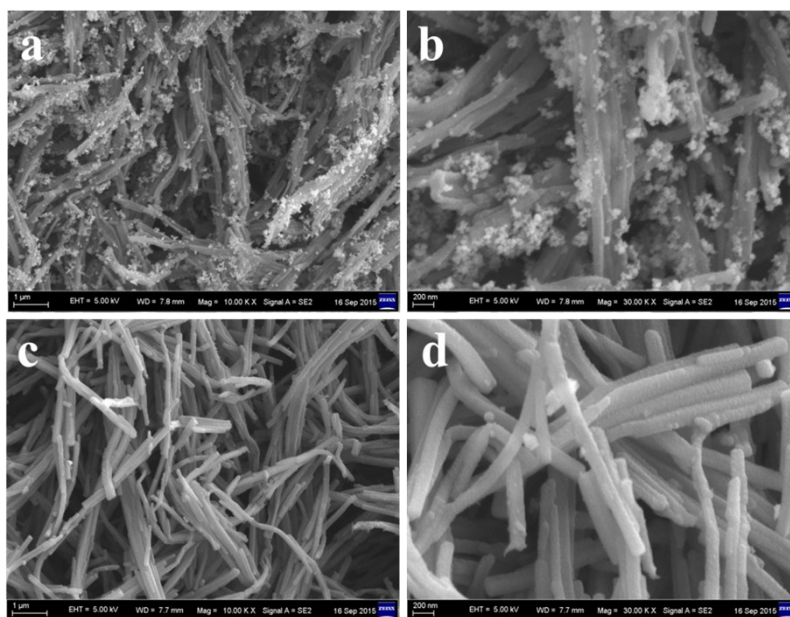


Figure S4. SEM of as-prepared Fe-PPy-MO (a,b) and PPy-MO (c,d).

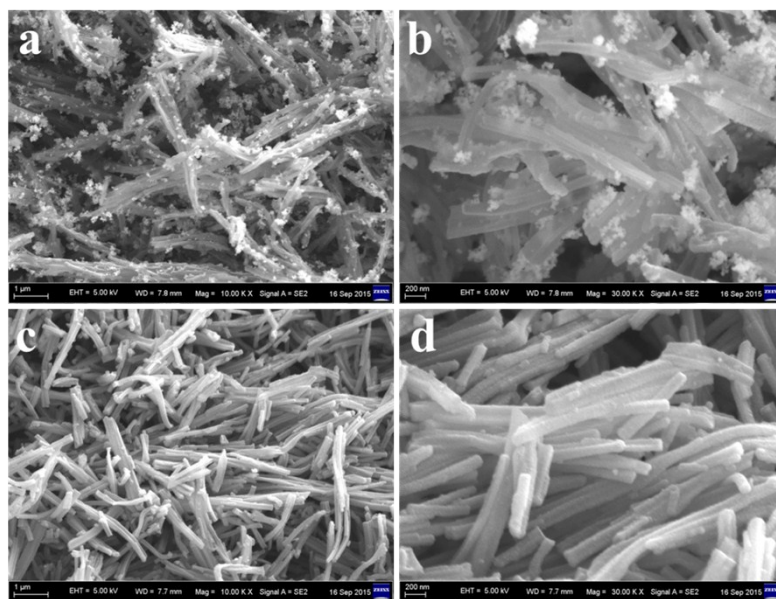


Figure S5. SEM images of Fe-PPy-MO (a,b) and PPy-MO (c,d) after annealed at 500 °C.

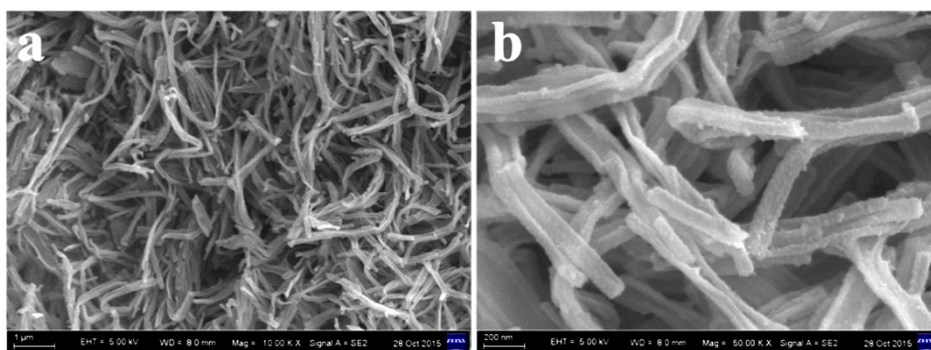


Figure S6. SEM images of NSCNT-800.

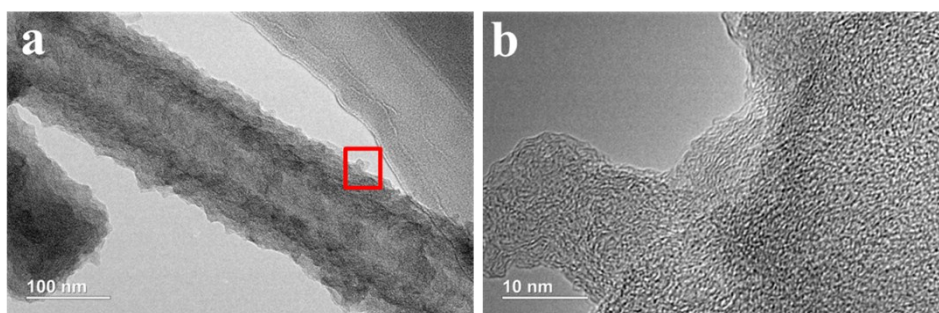


Figure S7. TEM images of NSCNT-800.

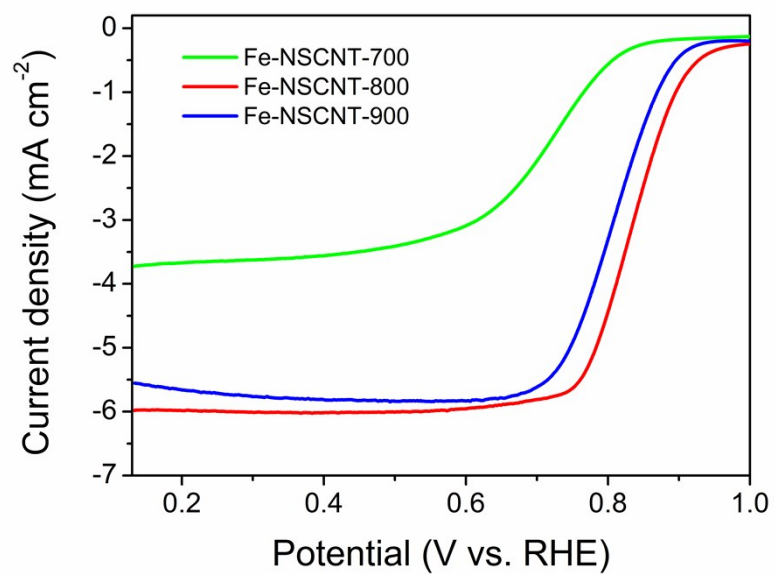


Figure S8. LSV curves of Fe-NSCNT-700, Fe-NSCNT-800 and Fe-NSCNT-900 in the O₂-saturated KOH (0.1 M) solution measured at a sweep rate of 10 mV s⁻¹ and an electrode rotation speed of 1600 rpm after background correction.

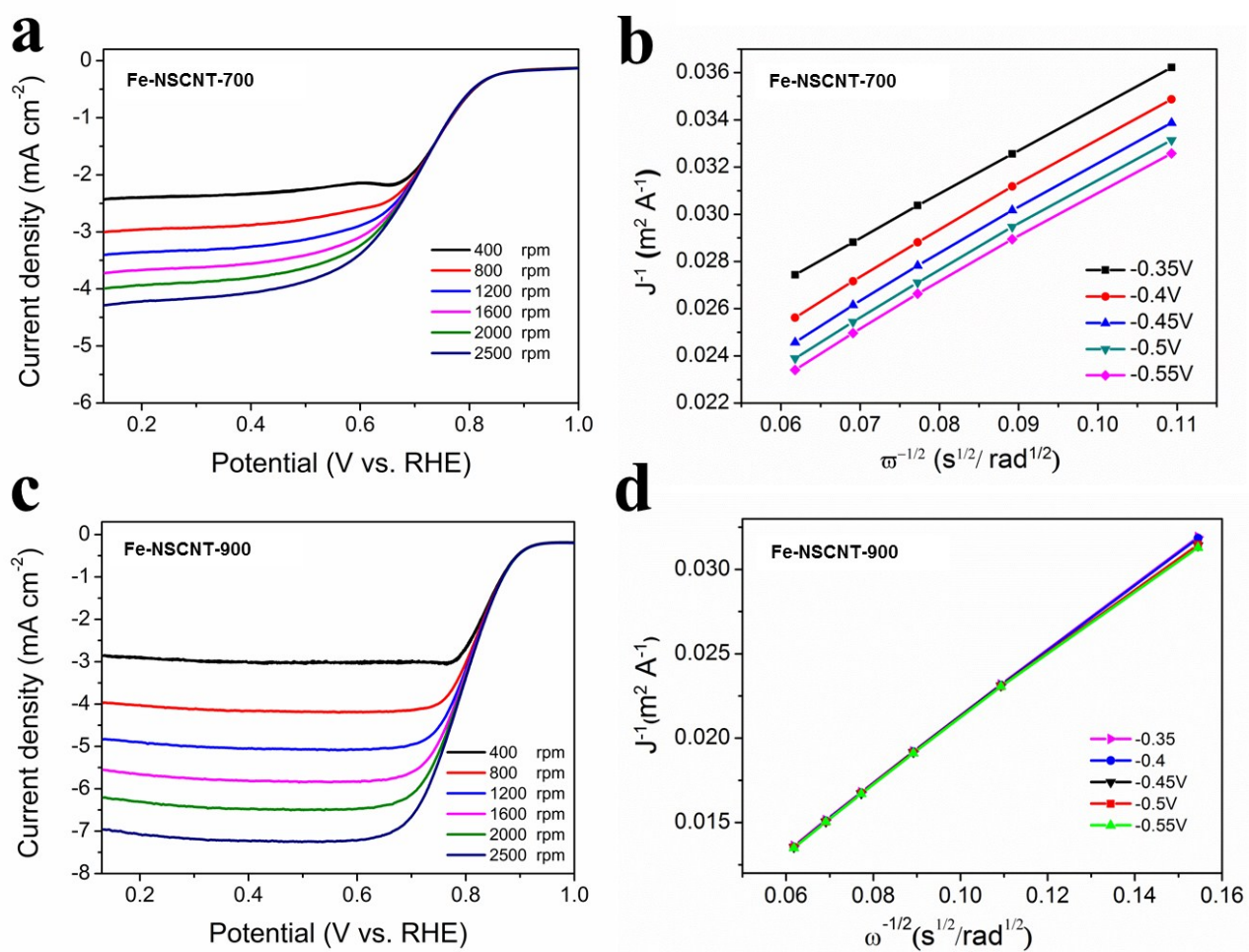


Figure S9. LSV curves and the corresponding Koutecky-Levich plots at different potentials of Fe-NSCNT-700 (a,b) and Fe-NSCNT-900 (c,d) in the O_2 -saturated KOH (0.1 M) solution after background correction, measured at a sweep rate of 10 mV s^{-1} and an electrode rotation speed of 1600 rpm.

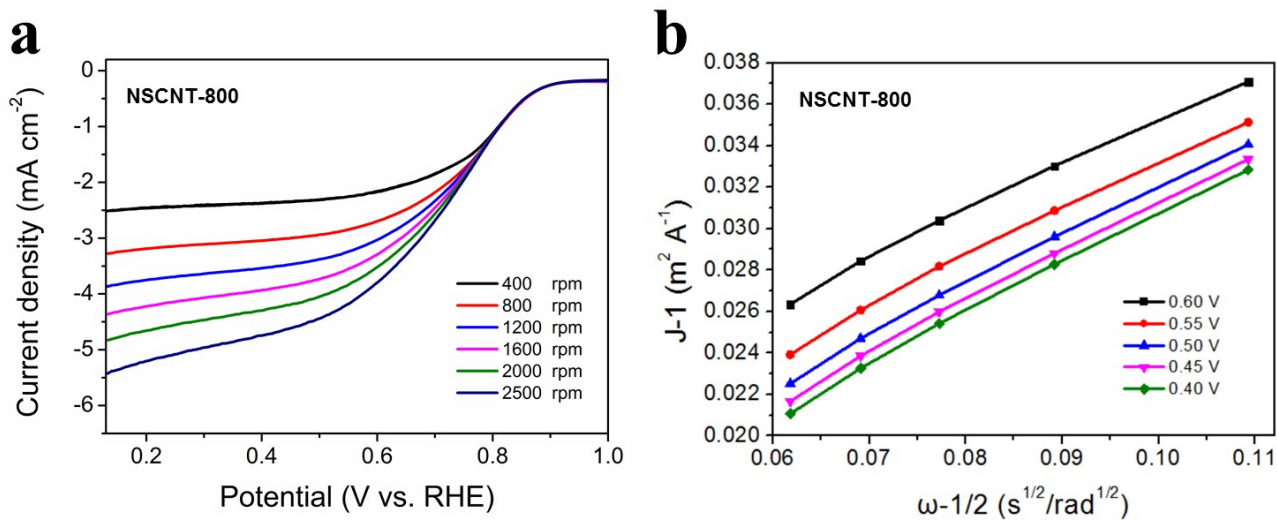


Figure S10. LSV curves (a) and the corresponding Koutecky-Levich plots at different potentials (b) of NSCNT-800 in the O_2 -saturated KOH (0.1 M) solution measured at a sweep rate of 10 mV s^{-1} and different electrode rotation speed after background correction.

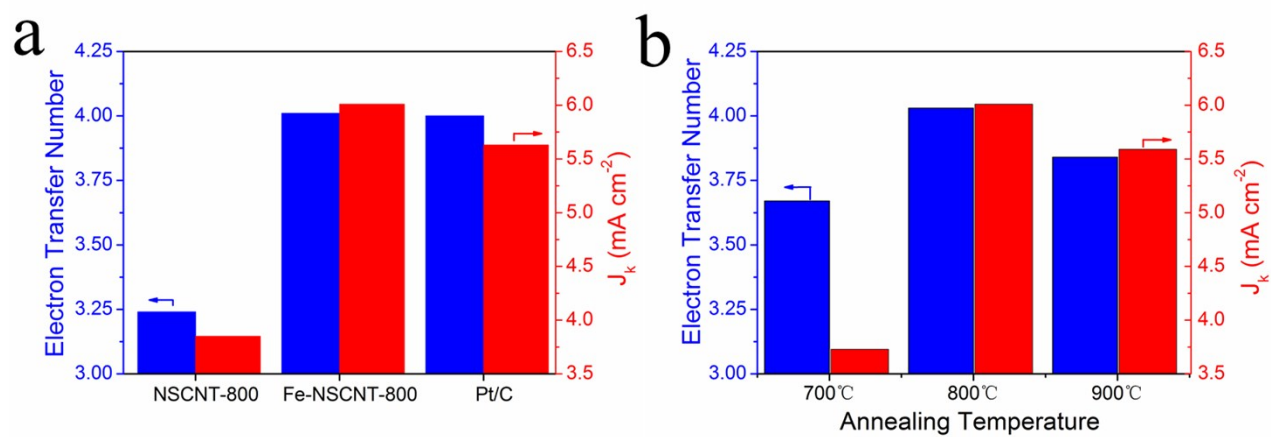


Figure S11. Comparison of electron transfer number and diffusion limiting current density among NSCNT-800, Fe-NSCNT-800 and 20% Pt/C (a), and the Fe-NSCNT catalysts fabricated with different temperature used at the last annealing step (b).

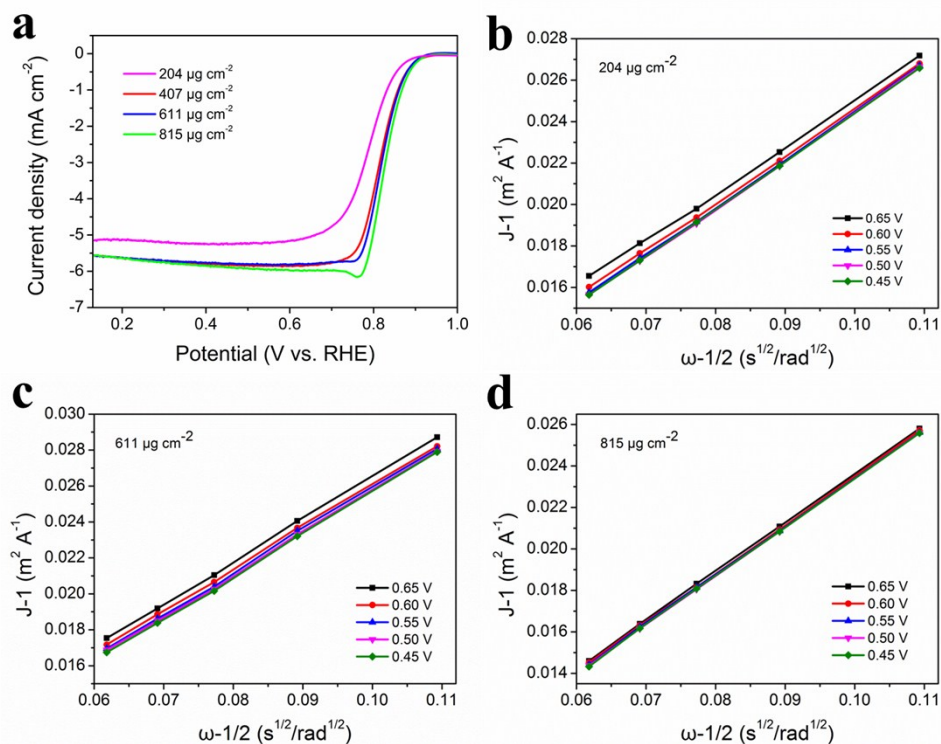


Figure S12. (a) ORR polarization curves of Fe-NSCNT-800 with different catalyst loading from 200 to 800 $\mu\text{g cm}^{-2}$ on the GC disk electrode of the RDE at a sweep rate of 10 mV s⁻¹ and the electrode rotation speed of 1600 rpm after background correction, the corresponding Koutecky-Levich plot of Fe-NSCNT-800 based on different catalyst loading of (b) 204 $\mu\text{g cm}^{-2}$, (c) 611 $\mu\text{g cm}^{-2}$, (d) 815 $\mu\text{g cm}^{-2}$.

Based on the RDE tests at different rotation speed and the corresponding Koutecky-Levich plots of Fe-NSCNT-800 with different catalyst loading, calculated using the Koutecky-Levich equations (eqs. 1-3, see Experimental section for details) after background correction, the electron transfer number (n) is 4.02, 3.94 and 3.87 for 204 $\mu\text{g cm}^{-2}$, 611 $\mu\text{g cm}^{-2}$ and 815 $\mu\text{g cm}^{-2}$ over the potential range from 0.6 - 0.40 V versus RHE, respectively. The loading experiments revealed that no matter the high loading or low loading, the electron-transfer number were all larger than 3.87.

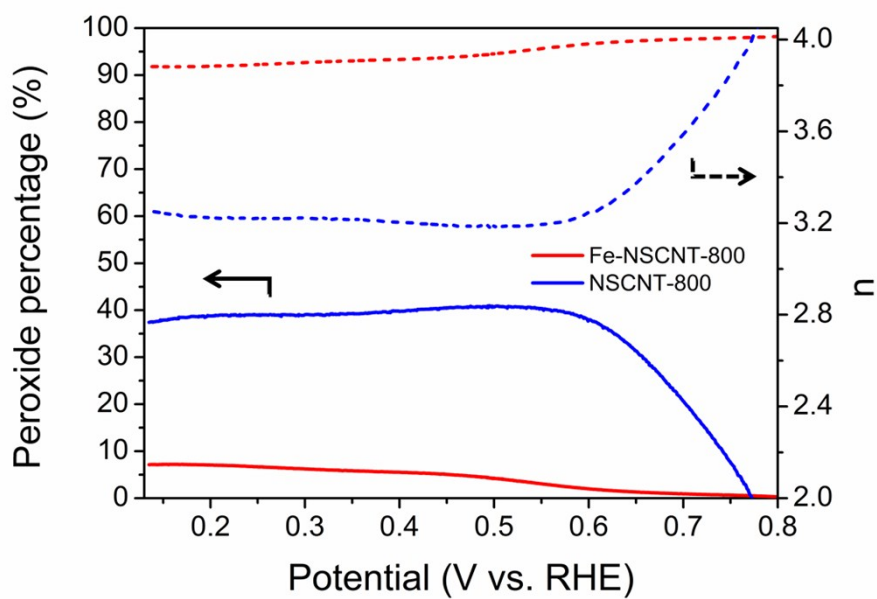


Figure S13. Percentage of peroxide (solid line) and the electron transfer number (n) (dash line) of Fe-NSCNT-800 and NSCNT-800 hybrids at various potentials, based on the corresponding RRDE data in Figure 3d.

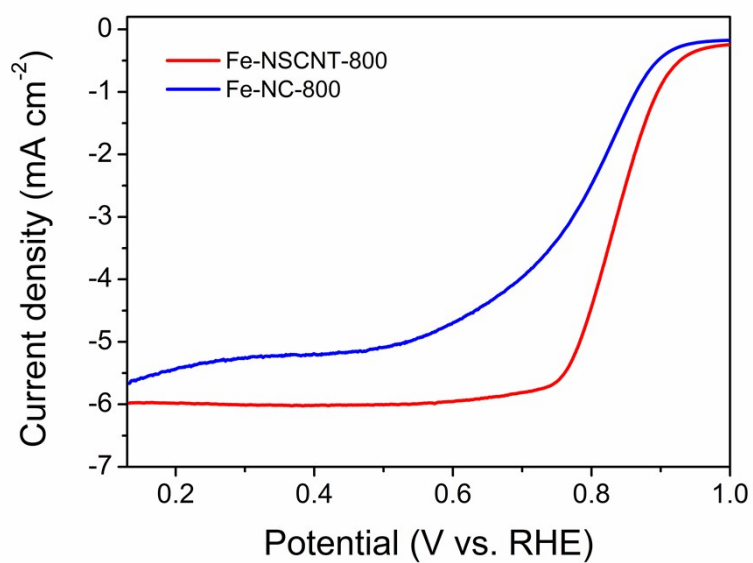


Figure S14. Linear sweep voltammetry (LSV) curves of Fe-NSCNT-800 and Fe-NC-800 in O₂-saturated KOH (0.1 M) solution at a sweep rate of 10 mV s⁻¹ and the electrode rotation speed of 1600 rpm after background correction.

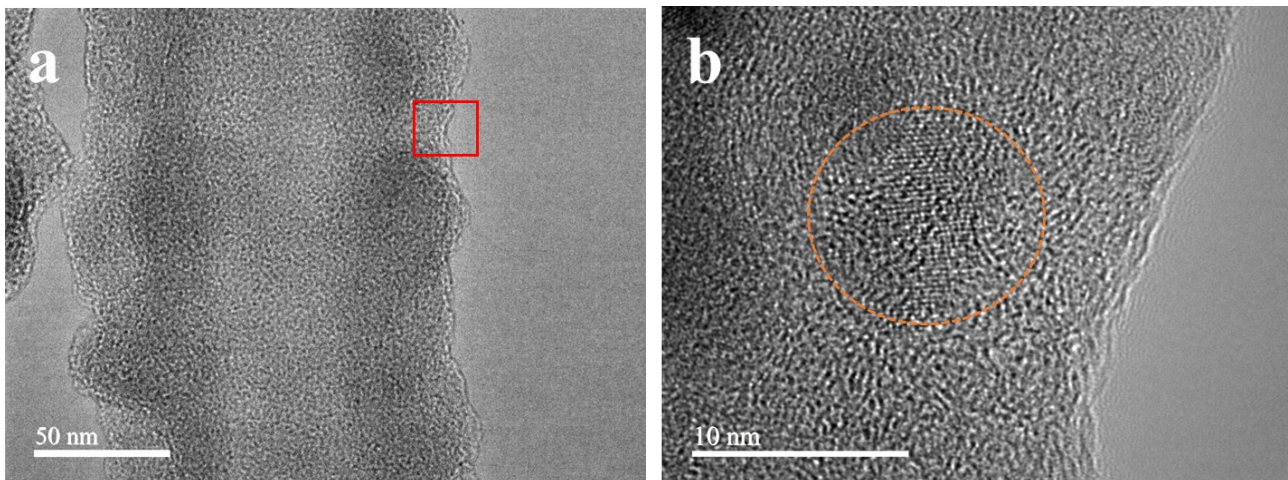


Figure S15. TEM images of Fe-NSCNT-800 after stability test of 10 hrs. Image (b) shows a magnified view of the red square in (a).

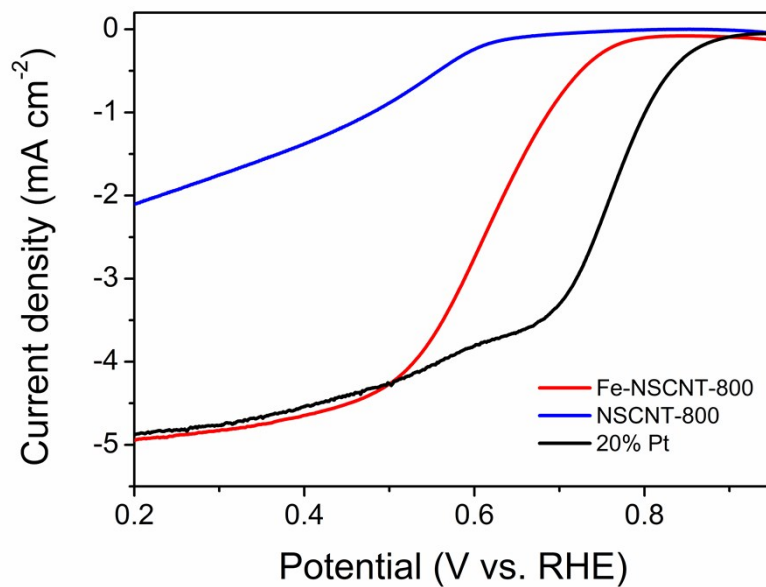


Figure S16. LSV curves of Fe-NSCNT-800, NSCNT-800 and 20% Pt/C in the O₂-saturated H₂SO₄ (0.5 M) solution measured at a sweep rate of 10 mV s⁻¹ and an electrode rotation speed of 1600 rpm after background correction.

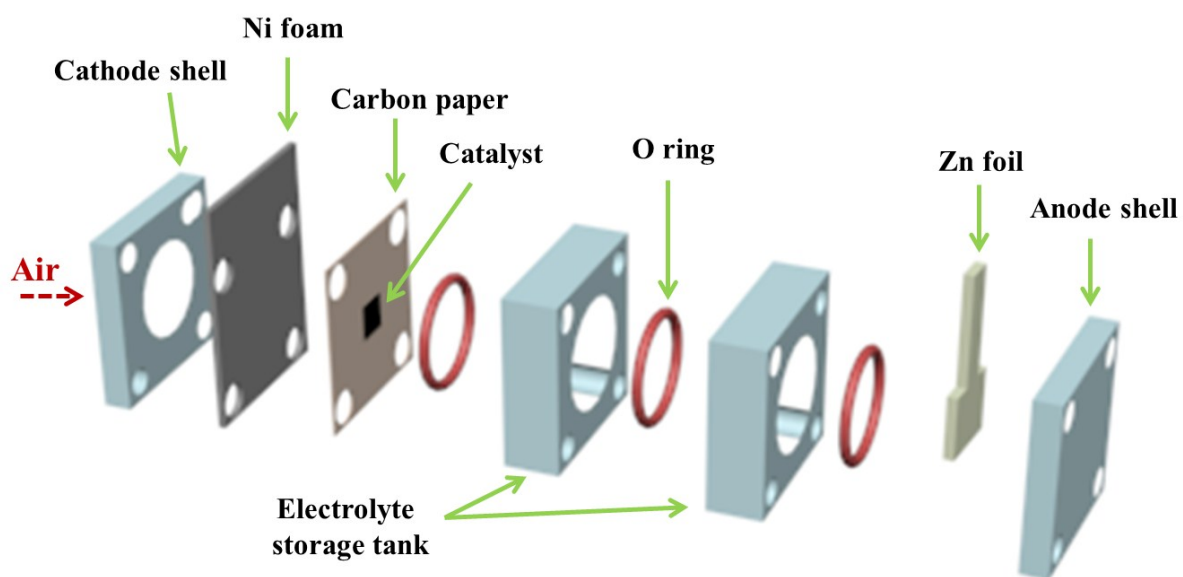


Figure S17. Schematic components diagram of the home-built Zinc-air cell.

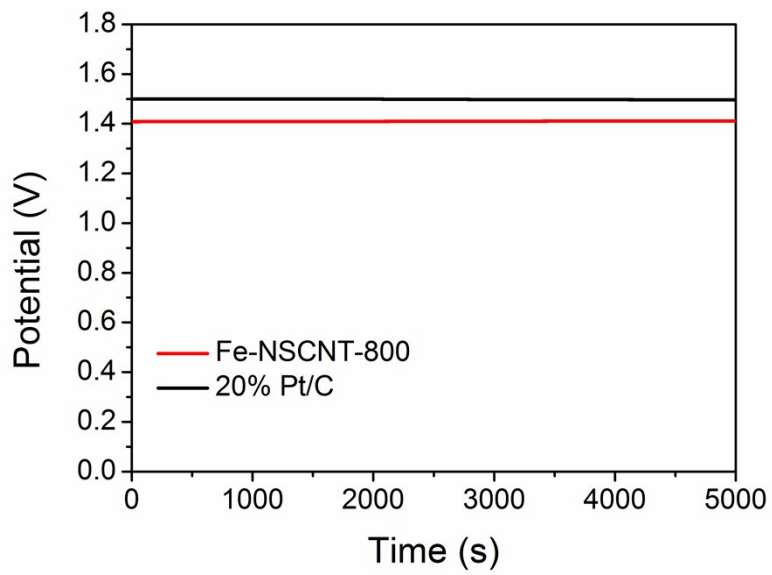


Figure S18. OCV of Zn-air batteries constructed using Fe-NSCNT-800 and 20% Pt/C